Supporting Information

Electronic and molecular structures of the active-site H-cluster in [FeFe]-hydrogenase determined by site-selective X-ray spectroscopy and quantum chemical calculations

Camilla Lambertz, Petko Chernev, Katharina Klingan, Nils Leidel, Kajsa G. V. Sigfridsson, Thomas Happe, and Michael Haumann

Details on sample preparation procedures.

Chlamydomonas reinhardtii [FeFe]-hydrogenase, HydA1(rai), was overexpressed heterologously in *Clostridium acetobutylicum* (strain ATCC 824), purified via Strep-Tag affinity chromatography with O_2-free buffer (100 mM Tris/HCl (pH 8.0), 2 mM sodium dithionite (NaDT)), and stored at -80 °C in the same buffer supplemented with 10 % (v/v) glycerol until use, as previously described.[1] Frozen CrHydA1 protein samples of several individual purifications were thawed, pooled, and concentrated (Amicon Ultracel 10 kDa, Millipore) up to 2 mM of protein. 20 µl of each protein sample was transferred using a Hamilton syringe into Kapton-covered acrylic-glass sample holders for XAE and stored in liquid nitrogen until use.

In parallel, i*n vitro* hydrogenase activity assays, using methylviologen as an electron donor[1] were performed regularly to guarantee a consistently high protein quality. All preparations showed a specific hydrogenase activity (H_2 evolution rate) of about 800 nmol H_2 min^{-1} µg $HydA1^{-1}$, which is similar to previously described activities.[2]

The apo-protein of the [FeFe]-hydrogenase, HydA1(apo), containing only the $[4Fe4S]_H$ unit, was obtained by protein overexpression in *E. coli* strain BL21 DE3 DiscR using a pET plasmid lacking the respective maturases (HydE, HydG, HydF) for assembling the active H-cluster structure.[3-4] Purification via a Strep-Tag was performed as outlined above. Immediately after purification, elution fractions containing the highest amount of protein were pooled and concentrated (Amicon Ultracel 10 kDa, Millipore) up to 600 µM and 20 µl of the sample was transferred to the XAE sample holders and stored in liquid nitrogen until use.

Clostridial ferredoxin, FDX(4Fe), was homologously overexpressed in *C. acetobutylicum*, purified as described elsewhere,[4] and concentrated twice (Vivaspin 2, 5 kDa, Satorius) up to 700 µM. Aliquots of 20 µl were transferred to the sample holders and stored in liquid nitrogen.

All purification and preparation steps were performed under strictly anaerobic conditions in an anaerobic tent. The purity of each protein sample was assayed routinely by SDS-polyacrylamide gel electrophoresis.

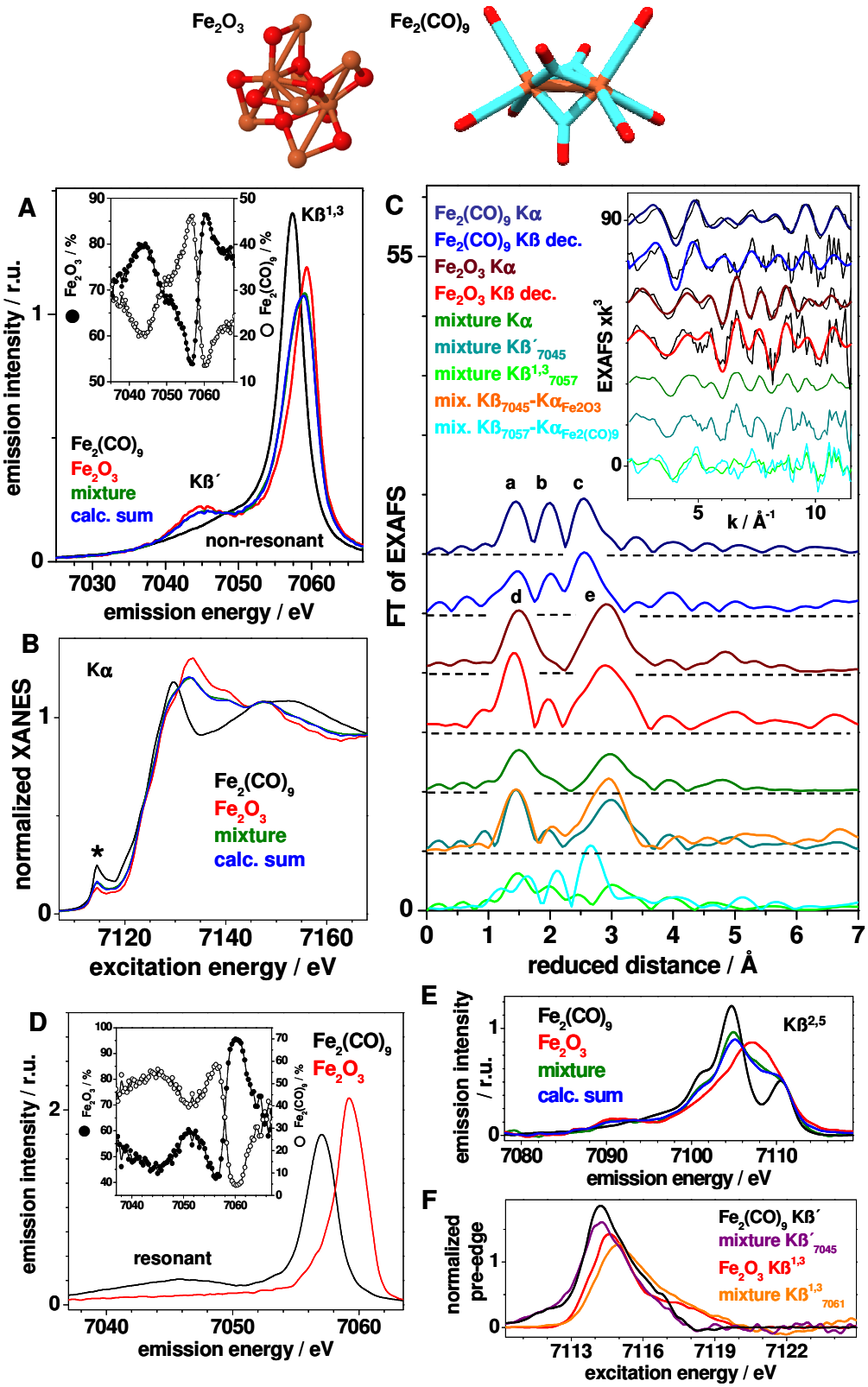

Figure S1: Spin- and site-selective XAE on a Fe_2O_3 and $Fe_2(CO)_9$ powder mixture. The mixture contained 70 % iron from Fe_2O_3 and 30 % iron from $Fe_2(CO)_9$, i.e. an iron site stoichiometry, which was similar to the one in the H-cluster (66.7 % *hs* iron in $[4Fe4S]_H$ and 33.3 % *ls* iron in $[2Fe]_H$). Top: crystal structures of Fe_2O_3[5] with mainly octahedral *hs* Fe(III) ions and $Fe_2(CO)_9$ with *ls* Fe(0)-$(CO)_6$ ligation.[6] Color code: orange, Fe; red, O; cyan, C. Bottom: (A) Kß emission spectra for non-resonant excitation of the individual compounds and the mixture and sum spectrum calculated by stoichiometrical weighting of the individual spectra. The relative contributions of the two compounds to the weighted-sum non-resonant

Kß spectrum as function of the emission energy are shown in the inset. (B) Kα-fluorescence detected XANES spectra as indicated. (C) Fourier-transforms (FTs) of EXAFS oscillations (in the inset) of the pure compounds for Kα-detection, of the mixture for Kß-detection at the indicated energies, and deconvoluted spectra for the pure species as derived from calculation of differences of stoichiometrically weighted Kß-detected spectra of the mixture (denoted "Kß dec.") or from calculation of difference spectra between stoichiometrically weighted Kß-detected spectra of the mixture and Kα-detected spectra of the pure species. Inset: thin lines, experimental data; thick lines, EXAFS simulations with parameters in Table S1. FT peak features denoted a-e are due to specific iron-ligand or Fe-Fe distances of the individual compounds and are also observed in the site-selective difference spectra. (D) Kß emission lines for resonant excitation at 7113.5 eV of Fe_2O_3 or at 7116.5 eV of $Fe_2(CO)_9$. The inset shows the relative contributions of the two compounds to the weighted-sum resonant-excitation Kß spectrum of the mixture as function of the emission energy. (E) $Kß^{2,5}$ emission lines (valence-to-core transitions) as indicated. (F) Pre-edge absorption spectra (core-to-valence transitions) measured at the indicated emission energies (Kß´, 7045 eV; $Kß^{1,3}$, 7059 eV) for the respective samples. Pre-edge spectra were isolated from the normalized XANES.

Table S1: EXAFS simulation parameters for reference compounds.[a]

sample	detection mode	Fe-C(=O)	Fe-O	Fe-S	Fe-Fe	R_F [%]
		N [per Fe ion] / R [Å] / $2\sigma^2$ x10^3 [Å^2]				
$Fe_2(CO)_9$	Kα EXAFS	6* / 1.85 / 33	-	-	1* / 2.47 / 3	30.7
	crystallography	6 / 1.83 / -	-	-	1 / 2.46 / -	-
	Kß EXAFS-dif.	6* / 1.85 / 36	-	-	1* / 2.48 / 12	31.5
Fe_2O_3	Kα EXAFS	-	6* / 1.98 / 16	-	6* / 2.99 / 21 6* / 3.42 / 16	26.2
	crystallography	-	3 / 1.94 / - 3 / 2.11 / -	-	6 / 2.95 / - 6 / 3.70 / -	-
	Kß EXAFS-dif.	-	6* / 1.93 / 9	-	6* / 2.97 / 23 6* / 3.40 / 13	38.4
$Fe(dedtc)_3$	Kα EXAFS	-	-	6* / 2.30 / 8	-	6.6
	$Kß^{1,3}{}_{7058}$ EXAFS	-	-	6* / 2.29 / 7	-	9.0
	$Kß´_{7045}$ EXAFS	-	-	6* / 2.29 / 8	-	13.5
	crystallography	-	-	6 / 2.31 / -	-	-
PDT(2Fe)	Kα EXAFS	2* / 1.74 / 4	-	3* / 2.22 / 22	1* / 2.44 / 8	9.9
	$Kß^{1,3}{}_{7059}$ EXAFS	2* / 1.75 / 3	-	3* / 2.21 / 20	1* / 2.45 / 8	7.9
	$Kß´_{7045}$ EXAFS	2* / 1.76 / 4	-	3* / 2.22 / 19	1* / 2.44 / 9	11.8
	crystallography	2 / 1.76 / -	-	3 / 2.24 / -	1 / 2.55 / -	-
FDX(4Fe)	Kα EXAFS	-	-	4* / 2.31 / 6	3* / 2.75 / 17	12.8

[a]Parameters correspond to fits of spectra in Fig. S1-C (bold lines; Kß-dec = Kß EXAFS-dif.) and Fig. S4. *N*, coordination number; *R*, interatomic distance, $2\sigma^2$, Debye-Waller parameter; R_F, weighted fit error sum. (*) Coordination numbers that were fixed in the fit procedures. $Fe(dedtc)_3$ contains *ls* $Fe(III)S_6$ sites at 20 K (dedtc = diethyldithiocarbamate);[7] PDT(2Fe) denotes the $(\mu\text{-pdt})[Fe(CO)_2(PMe_3)]_2$ complex (pdt = $SCH_2CH_2CH_2S$) in Fig. S2;[8] FDX(4Fe) denotes purified ferredoxin protein from *C. acetobutylicum* containing two [4Fe4S] clusters.[9] The EXAFS simulation of the deconvoluted Fe_2O_3 spectrum (Kß-EXAFS-dif.) revealed a similar bias for shorter Fe-Fe distances in the Kß´-detected EXAFS as found for the H-cluster. For further details see the text.

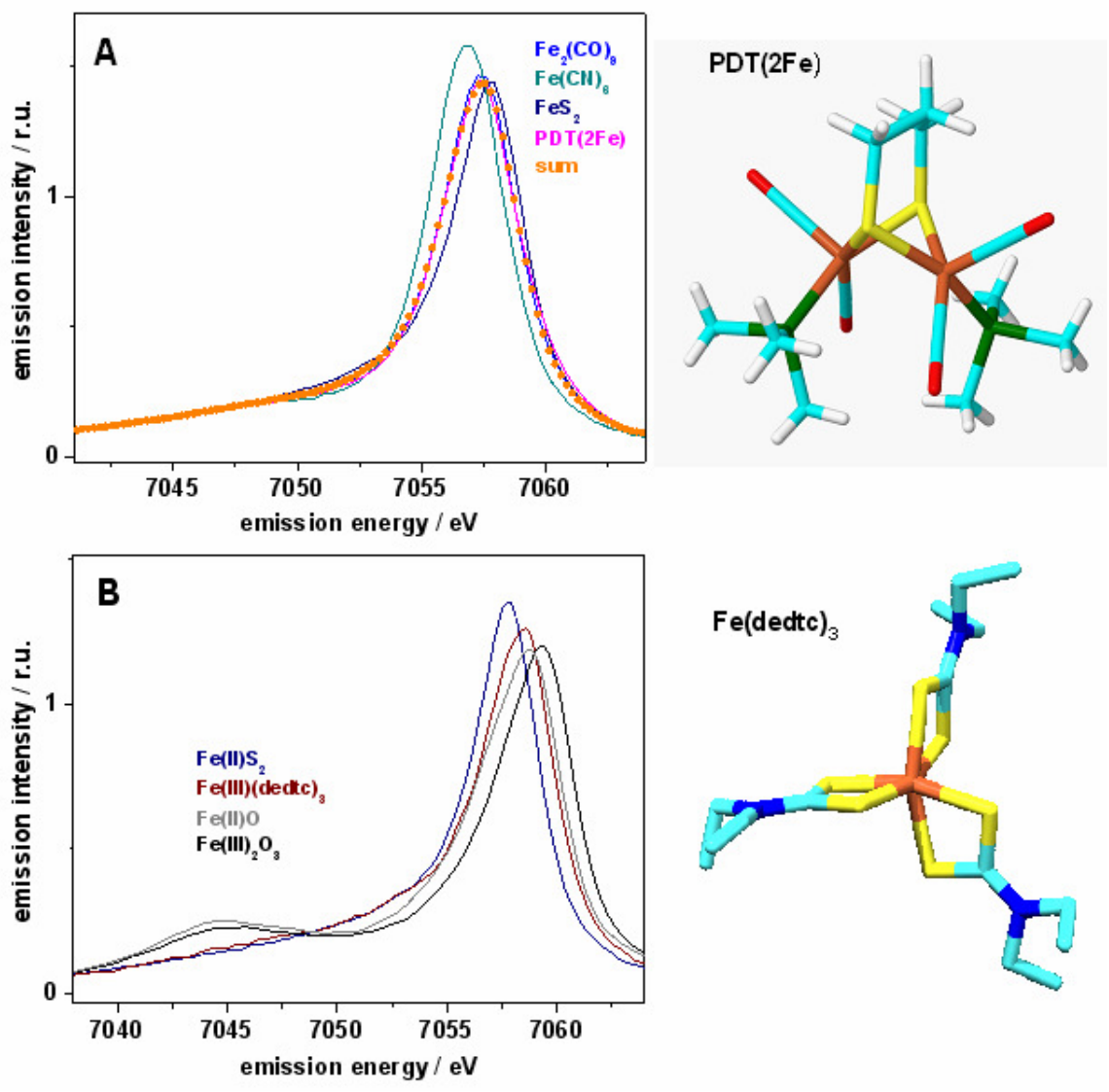

Figure S2: Kß emission spectra of iron reference compounds. (A) Summation (sum) of spectra of the indicated iron compounds with only a single ligand species at the metal, which were weighted according to the ligand stoichiometry in PDT(2Fe), reproduced the Kß emission spectrum of PDT(2Fe) well. (B) A shift to higher energies for the Kß^{1,3} maximum is observed for a Fe(II)→Fe(III) transition in *ls* FeS_6 sites (in iron disulfide, $Fe^{II}S_2$, and $Fe^{III}(dedtc)_3$) and in *hs* FeO_6 sites (in $Fe^{II}O$ and $Fe^{III}{}_2O_3$). The crystal structures of PDT(2Fe)[8] and $Fe(dedtc)_3$ (see Table S1 for interatomic distances) are shown on the right (Fe, orange; S, yellow; C, cyan; P, green; O, red; N, blue; H, white). Protons were omitted in the drawing of $Fe(dedtc)_3$.

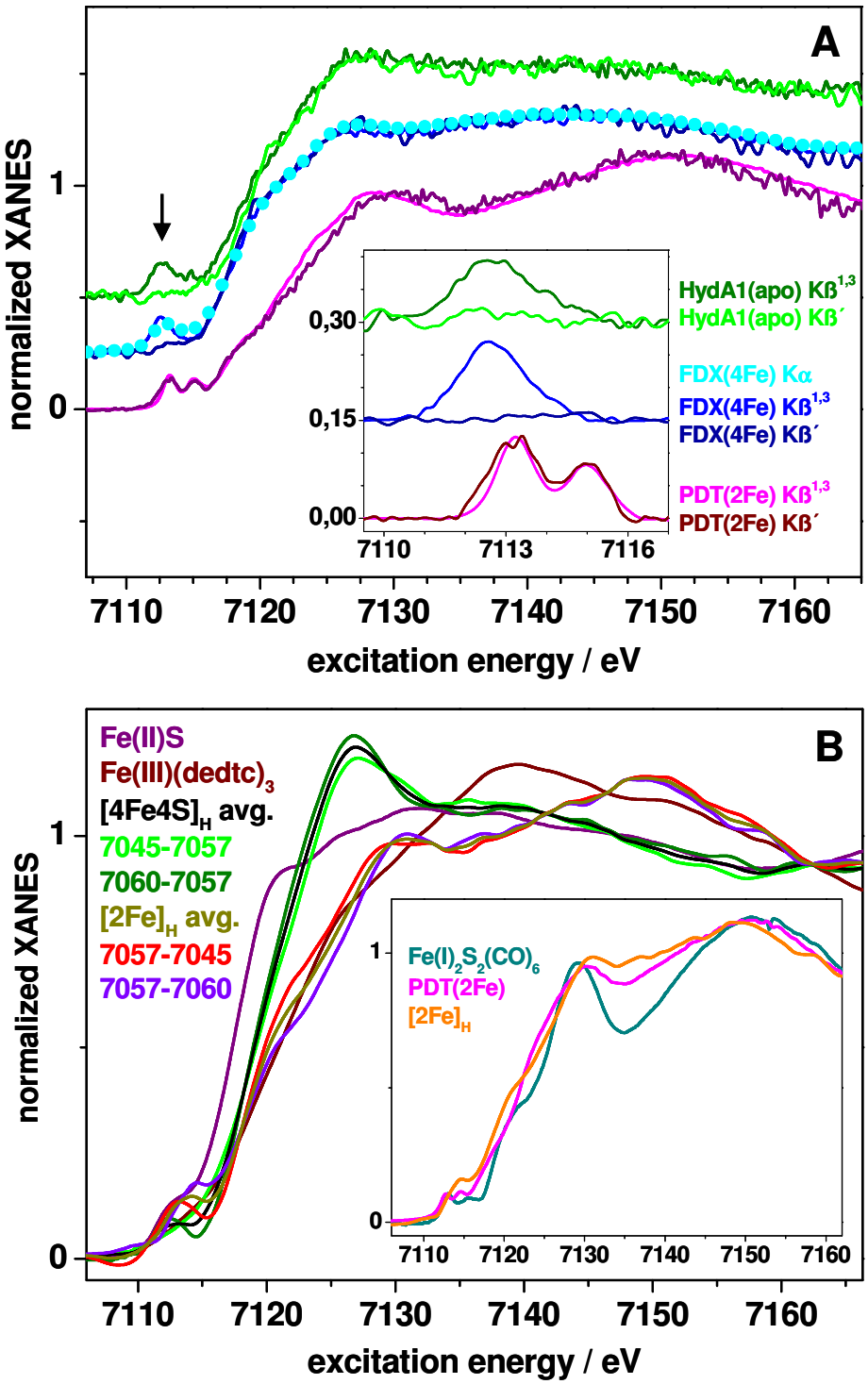

Figure S3: XANES spectra of proteins and reference compounds. (A) Comparison of Kα- and Kß-detected (Kß´, 7045 eV; Kß^{1,3}, ~7058 eV) spectra and corresponding isolated pre-edge features (arrow) in the inset. Data in the inset emphasize the high spin-selectivity of the Kß´ and Kß^{1,3} spectral regions for resonant excitation into the pre-edge. (B) Kß-detected spectra (at ~7058 eV) for the indicated reference compounds and for $[4Fe4S]_H$ and $[2Fe]_H$ as obtained by calculation of the weighted differences of spectra for Kß-detection at the indicated energies (see the legend of Fig. 4 for the scaling factors) and the respective averaged spectra (avg.). The inset shows the Kß^{1,3}-detected (at ~7058 eV) XANES of the indicated complexes. For further details see the text.

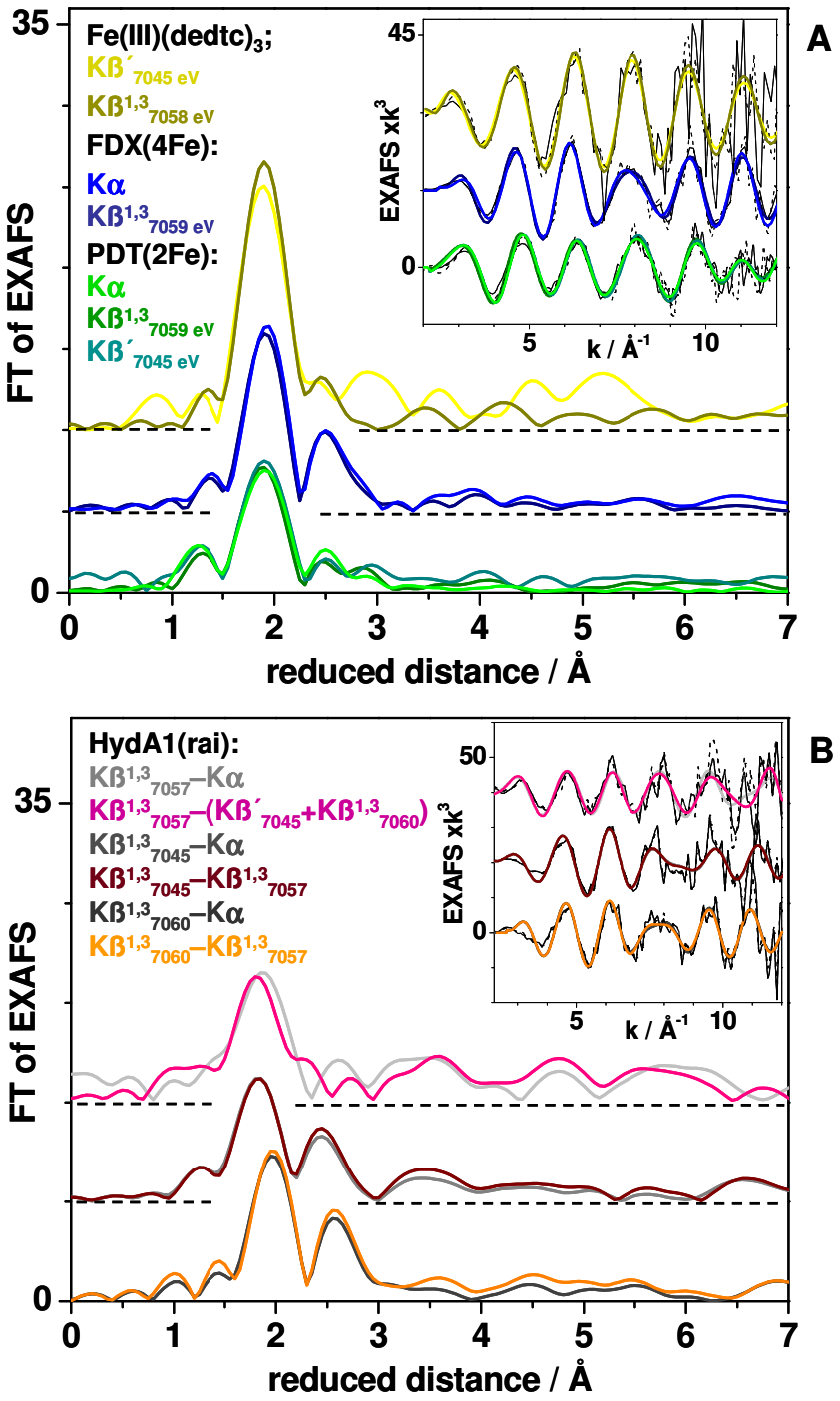

Figure S4: EXAFS spectra of proteins and reference compounds. (A) Fourier-transforms (FTs) of the EXAFS oscillations in the inset for the indicated compounds and detection modes (compare Fig. S3). Thin lines, experimental data; thick lines, simulations with parameters in Table S1. (B) Spectra of HydA1(rai) as derived from calculation of weighted differences of Kß- and Kα- or Kß-detected spectra at the indicated energies. The top two spectra correspond to the $[2Fe]_H$ unit and the two middle and two bottom spectra to the $[4Fe4S]_H$ unit for Kß´ (7045 eV) or $Kß^{1,3}$ (7060 eV) detection. For scaling factors in the spectral difference calculations using Kß-detected spectra see the legend of Fig. 4. Difference spectra involving Kα-detected spectra were obtained as follows: $[4Fe4S]_H$ = {$(HydA1(rai)_{7045}$-$HydA1(rai)_{Kα}$x0.69)x3.22 + $(HydA1(rai)_{7060}$-$HydA1(rai)_{kα}$0.72)x3.57} /2; $[2Fe]_H$ = $(HydA1(rai)_{7057}$-$HydA1(rai)_{Kα}$x0.75)x4.00). Inset: thin lines, experimental data; thick lines, simulations with parameters in Table 1. For further details see the text.

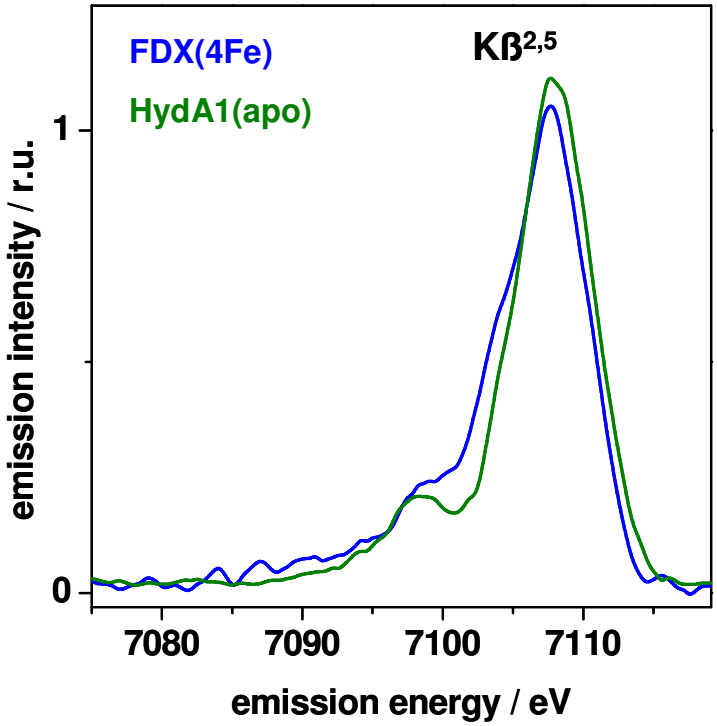

Figure S5: Valence-to-core emission spectra for HydA1(apo) and FDX(4Fe). Kß^{2,5} spectra were normalized to unity area in the shown spectral region.

Table S2: Coordinates of the H-cluster model structure in Fig. 6.[a]

H	0.412	3.090	-1.660	N	2.062	-2.619	-2.117
H	-4.715	3.709	-1.644	C	0.613	-2.644	-2.158
H	-1.730	-3.817	-5.587	C	2.623	-1.301	-1.916
H	-0.861	2.197	-8.218	O	-2.766	0.446	0.743
H	2.380	-3.234	-1.358	N	0.695	2.787	1.099
C	-2.622	-4.194	-5.073	O	-0.029	-0.194	3.041
S	-4.104	-3.183	-5.515	N	0.021	-4.323	2.665
H	-2.446	-4.166	-3.991	O	3.511	-2.083	3.000
H	-2.803	-5.234	-5.379	C	-1.657	0.244	0.415
C	-5.251	2.882	-1.163	C	0.438	1.715	0.673
S	-6.247	1.953	-2.414	C	0.317	-0.647	1.990
H	-4.523	2.218	-0.684	C	0.470	-3.393	2.085
H	-5.932	3.279	-0.397	C	2.594	-2.033	2.247
C	-1.566	3.036	-8.263	Fe3	-3.568	-1.093	-4.948
S	-3.281	2.449	-7.960	Fe4	-4.525	1.138	-3.646
H	-1.271	3.782	-7.514	Fe1	-1.930	0.645	-3.606
H	-1.514	3.494	-9.261	Fe2	-3.260	1.369	-5.965
C	0.861	2.306	-2.278	S	-2.954	2.649	-4.058
S	-0.154	0.781	-2.185	S	-1.604	-0.231	-5.733
H	1.855	2.067	-1.881	S	-5.192	0.334	-5.695
H	0.931	2.633	-3.323	S	-3.437	-0.646	-2.674
Fep	0.000	0.000	0.000	H	0.264	-1.928	-2.914
Fed	1.259	-1.953	1.171	H	0.280	-3.654	-2.432
S	2.357	-0.485	-0.246	H	2.199	-0.624	-2.672
S	-0.292	-2.270	-0.563	H	3.715	-1.348	-2.033

[a]Fe_p and Fe_d denote the proximal and distal iron atoms in $[2Fe]_H$, Fe1,2,3,4 the iron atoms in $[4Fe4S]_H$ (see Fig. 6).

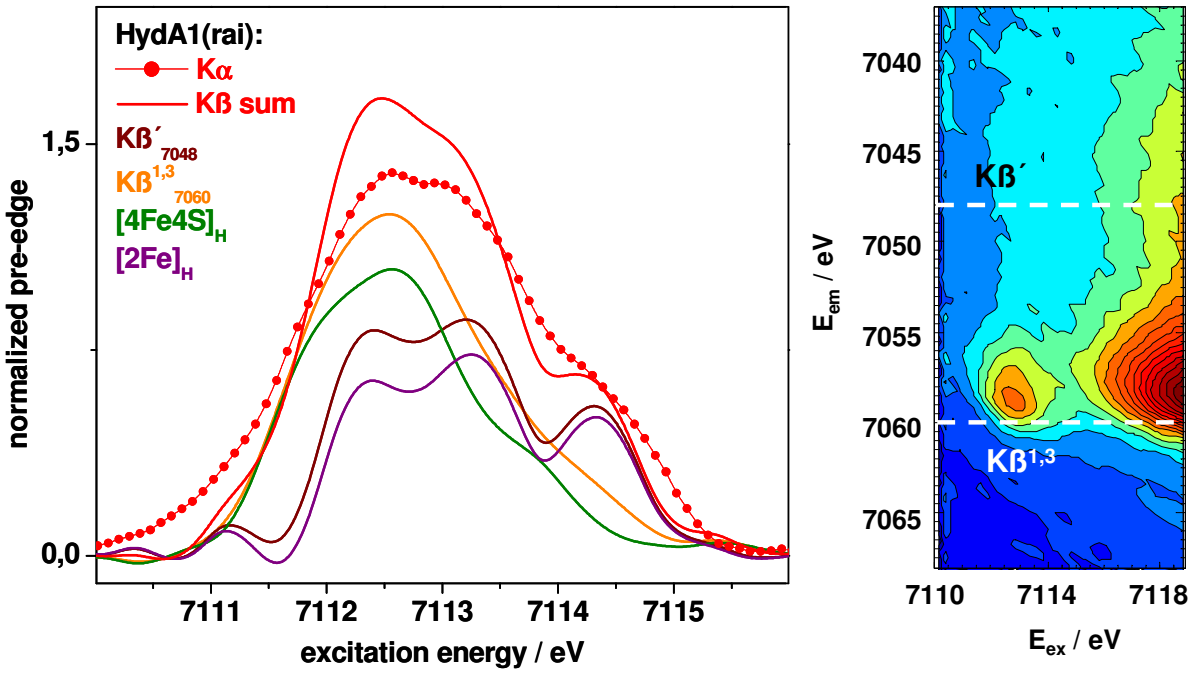

Figure S6: Site-selective pre-edge absorption spectra for HydA1(rai). Left: isolated pre-edge spectra for the indicated Kß-detection energies, summed Kß-detected spectrum, and Kα-detected spectrum, compared to the deconvoluted Kß´- and $Kß^{1,3}$-detected spectra at the indicated energies attributed to $[2Fe]_H$ and $[4Fe4S]_H$. For scaling factors in the calculation of pure spectra see the legend of Fig. 5. Kß-detected spectra were derived from transects at constant emission energy (dashed white lines, spectral width of ±1 eV) through the resonant inelastic scattering plane (RIXS) data shown on the right as a contour plot (the gradient from blue to red colours denotes changes from lower to higher emission intensities). Pre-edge spectra were isolated by subtraction of the main edge background by a polynomial spline.

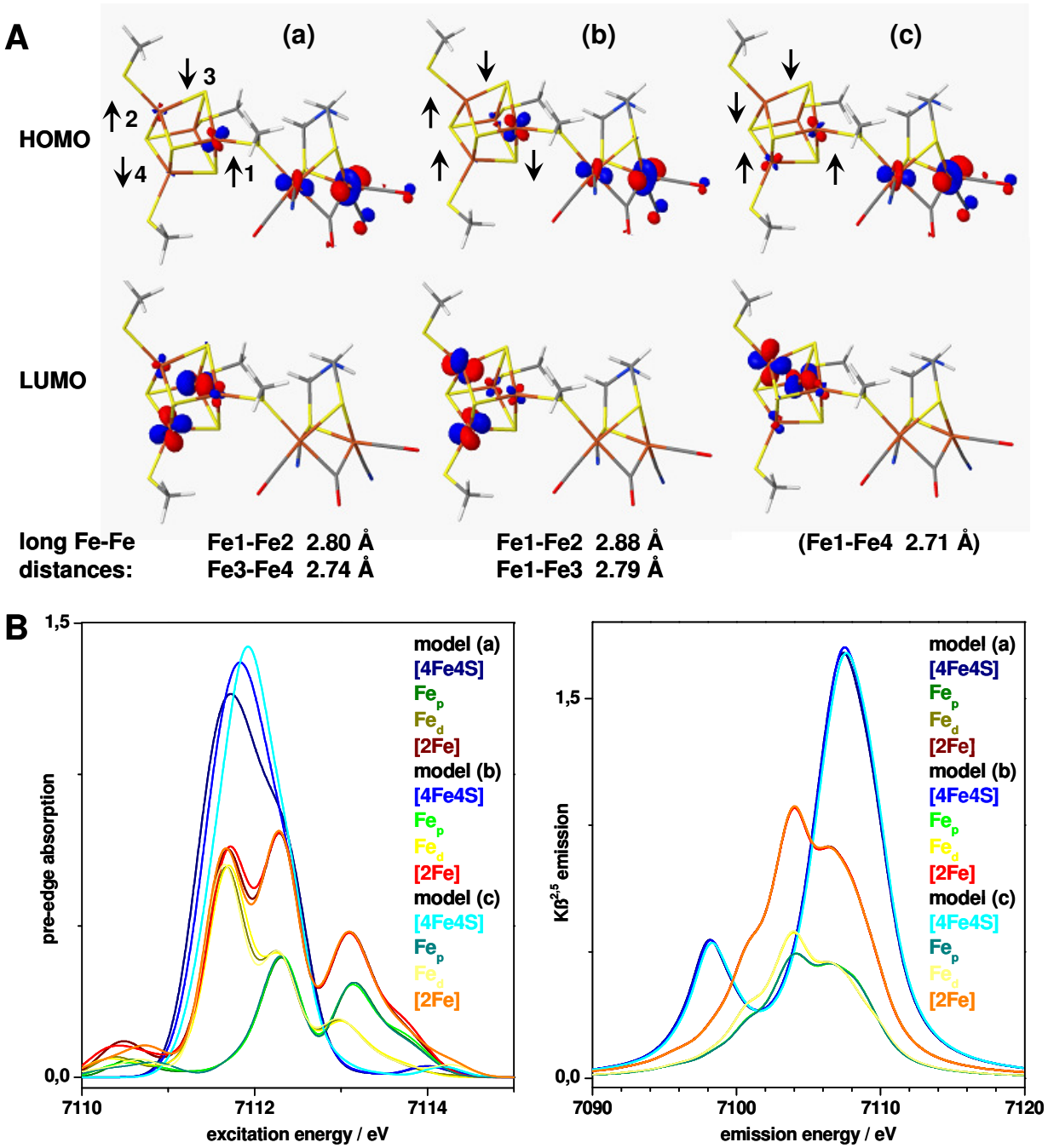

Figure S7: Structures and XAE spectra for alternative spin configurations. (A) Structures and HOMO/LUMO configurations from DFT for three different net spin orientations (arrows) on the iron atoms in $[4Fe4S]_H$. The overall structures were similar, but the longer Fe-Fe distances were observed between different Fe ions in (a) and (b). Structure (c) showed only one Fe-Fe distance, which was slightly longer than the other 5 Fe-Fe distances in the cubane. Both irons in $[2Fe]_H$ carried almost zero (≤0.17) spins in all structures, indicating spin pairing of the formal Fe(I) ions. The Fe-Fe distance in $[2Fe]_H$ were identical (2.59 Å) in all structures. Structures (a) and (c) were almost identical (ΔE <2 meV) in energy, whereas structure (b) was slightly (31.5 meV) lower in energy than (a). (B) Calculated pre-edge absorption (left) and $Kß^{2,5}$ emission (right) spectra for the structures in (A). The pre-edge spectra of $[4Fe4S]_H$ were rather similar, but the more pronounced high-energy shoulder for (a) compared to the rather featureless spectra of (b) and (c) seemingly was better in agreement with the experimental data (Fig. 5). The $Kß^{2,5}$ spectra for $[4Fe4S]_H$ were practically identical. The pre-edge absorption and $Kß^{2,5}$ emission spectra for $[2Fe]_H$ were almost identical for all structures, as were the individual spectra for Fe_p and Fe_d. The calculated LUMO-HOMO energy differences were small for all structures, i.e. 0.17 eV for (a), 0.21 eV for (b), and 0.07 eV for (c).

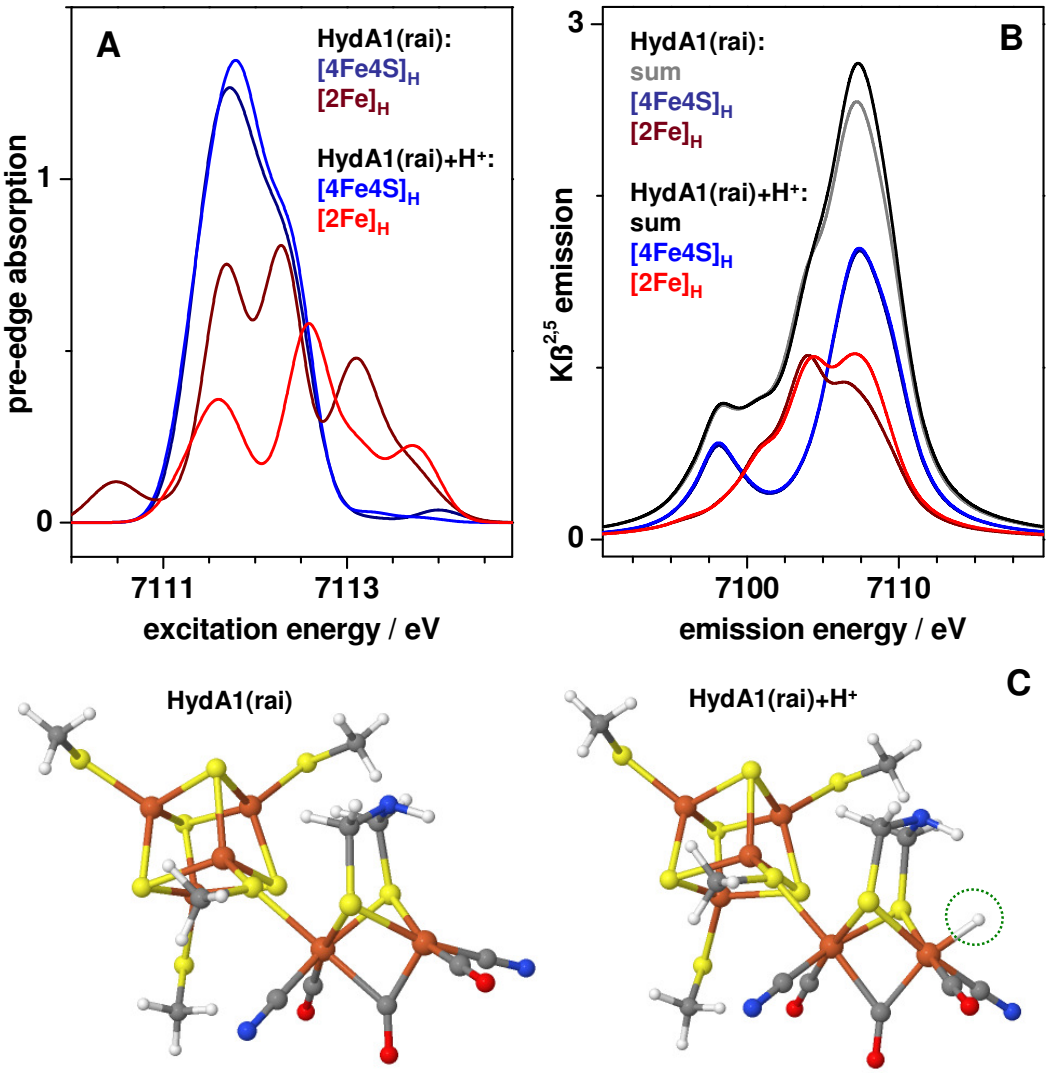

Figure S8: Comparison of unprotonated and protonated H-cluster structures. DFT-calculated pre-edge absorption spectra (A) and Kß^{2,5} emission spectra (B) for H-cluster models (C) comprising formal $Fe^{II}_2Fe^{III}_2$-$2Fe^{I}$ states and either an open coordination site (C, left) at Fe_d or an additional proton (C, right, dotted circle) bound to Fe_d are shown. The calculated spectra for the unprotonated structure were in significantly better agreement with the experimental spectra of $[4Fe4S]_H$ and $[2Fe]_H$ (Fig. 5) than the spectra for the protonated structure. This supported the presence of an open coordination site at Fe_d in the reduced state, HydA1(rai).

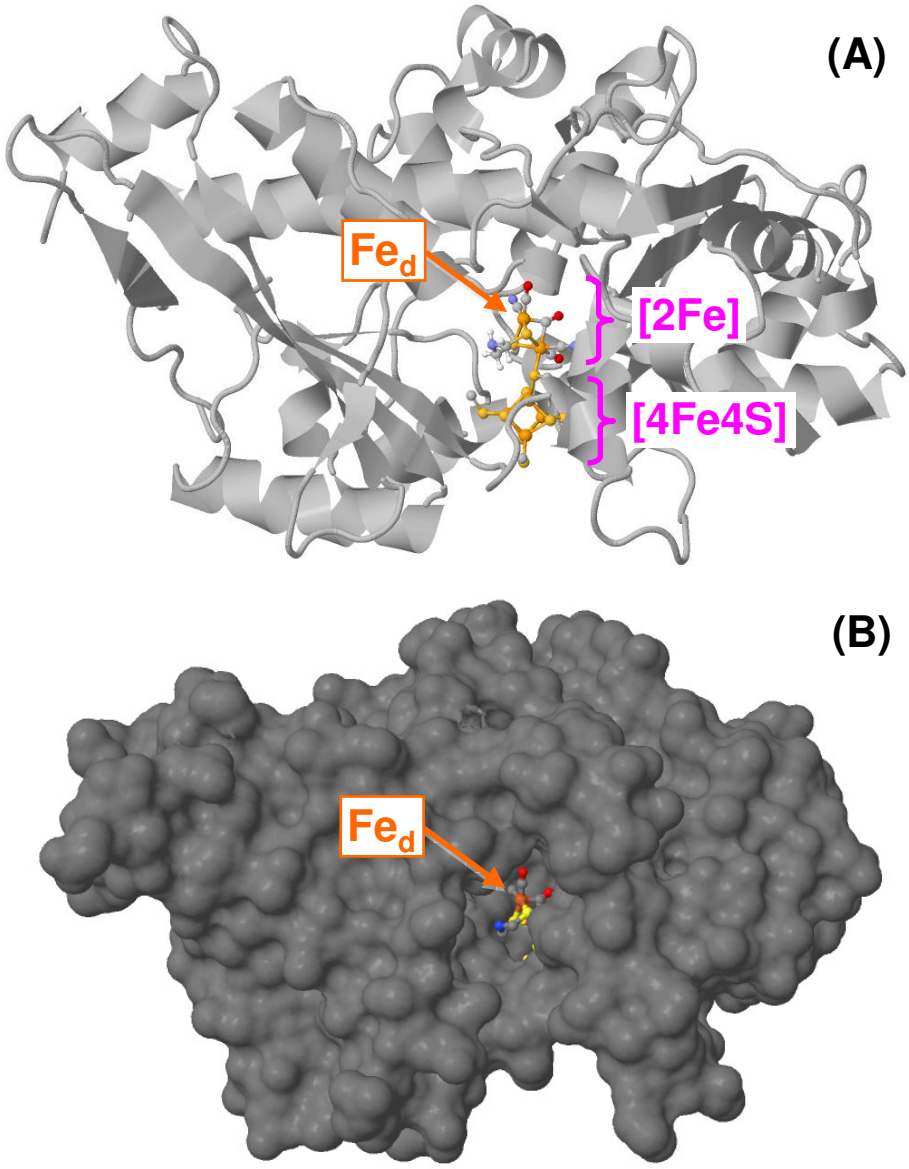

Figure S9: The H-cluster model in the HydA1 crystal structure. The $[4Fe4S]_H$ unit, the acetate molecule, and the Cl^- ion in the active site cavity in the crystal structure of apo-HydA1[10] were replaced by our H-cluster model from DFT (Fig. 6) to result in an orientation of the complex relative to the amino acid environment similar to the one in crystal structures of bacterial [FeFe]-hydrogenases.[11-13] The insertion required displacement of the iron atoms of $[4Fe4S]_H$ by <1 Å compared to the apo-HydA1 structure to yield chemically reasonable distances between $[2Fe]_H$ and the neighboring atoms. (A) H-cluster in ball-and-stick and protein in ribbon representations. (B) H-cluster in ball-and-stick and protein in space-filling representations. The distal iron atom (Fe_d) of $[2Fe]_H$ is visible in (B) and thus accessible for, e.g., proton or O_2 binding from the bulk phase. $[4Fe4S]_H$ is exposed to the opposite side of the protein (not shown) where the electron-donating ferredoxin (PetF) supposedly binds.[14]

Supporting References

(1) von Abendroth, G.; Stripp, S.; Silakov, A.; Croux, S.; Soucaille, S.; Girbal, L.; Happe, T. *J. Hydrogen Energ.* **2008**, *33*, 6076-6081.
(2) Happe, T.; Naber, J. D. *Eur. J. Biochem.* 1993, *214*, 475-581.
(3) Silakov, A.; Wenk, B.; Reijerse, E.; Lubitz, W. *Phys. Chem. Chem. Phys.* **2009**, *11*, 6592-6599.
(4) Kuchenreuther, J. M.; Grady-Smith, C. S.; Bingham, A. S.; George, S. J.; Cramer, S. P.; Swartz, J. R. *PLoS One* **2010**, *5*, e15491.
(5) Blake, R. L.; Hessevic.Re; Zoltai, T.; Finger, L. W. *Am. Mineral.* **1966**, *51*, 123-129.
(6) Cotton, F. A.; Troup, J. M. *J. Chem. Soc. Dalton Trans.* **1974**, 800-802.
(7) Leipoldt, J. G.; Coppens, P. *Inorg. Chem.* **1973**, *12*, 2269-2274.
(8) Leidel, N.; Hsieh, C. H.; Chernev, P.; Sigfridsson, K. G.; Darensbourg, M. Y.; Haumann, M. *Dalton Trans.* **2013**, *42*, 7539-7554.
(9) Noth, J.; Krawietz, D.; Hemschemeier, A.; Happe, T. *J. Biol. Chem.* **2013**, *288*, 4368-4377.
(10) Mulder, D. W.; Boyd, E. S.; Sarma, R.; Lange, R. K.; Endrizzi, J. A.; Broderick, J. B.; Peters, J. W. *Nature* **2010**, *465*, 248-251.
(11) Peters, J. W.; Lanzilotta, W. N.; Lemon, B. J.; Seefeldt, L. C. *Science* **1998**, *282*, 1853-1858.
(12) Nicolet, Y.; Lemon, B. J.; Fontecilla-Camps, J. C.; Peters, J. W. *Trends Biochem. Sci.* **2000**, *25*, 138-143.
(13) Nicolet, Y.; Piras, C.; Legrand, P.; Hatchikian, C. E.; Fontecilla-Camps, J. C. *Structure* **1999**, *7*, 13-23.
(14) Winkler, M.; Esselborn, J.; Happe, T. *Biochim. Biophys. Acta* **2013**, *1827*, 974-985.